ATLAS NOTE

ATL-PHYS-COM-2008-xxx

December 11, 2008

Use of Tracks to Reconstruct Jets in Damaged Calorimeter Regions

Georgios Choudalakis,* Eric Feng†

Enrico Fermi Institute and Department of Physics
University of Chicago
5640 S. Ellis Avenue
Chicago, IL 60637

Abstract

We study the use of tracks to reconstruct jets when part of the ATLAS Calorimeter is damaged. We first examine the purity and efficiency of reconstructing truth-level jets as track jets in different scenarios of calorimeter damage. We then combine information from the operational part of the calorimeter and the tracks in order to estimate the hadron-level ("truth-level") momentum of reconstructed jets. Only Monte Carlo events are used in this study.

*Electronic address: `Georgios.Choudalakis@cern.ch`
†Electronic address: `Eric.Feng@cern.ch`

Contents

1 Introduction

During operation, portions of the ATLAS Calorimeter may be non-functional. For example, the readout of a Tile Calorimeter [1] module ($\Delta\phi = \frac{\pi}{32}$) or a high voltage power supply in the Liquid Argon Calorimeter [2] ($\Delta\phi = \frac{\pi}{8}$) could fail. Such a scenario would negatively impact both the reconstruction efficiency of a hadronic jet in the problematic region as well as the measurement of its momentum.

One possible solution is to identify jets by clustering tracks from the Inner Detector [3]. This has the advantage of being independent of the calorimeter. In this article we demonstrate the efficiency and purity of track jets with respect to truth jets, comparing their performance to that of calorimeter jets. We also use the track jets to estimate the hadron-level ("true") jet momentum. However, while the constituent track momenta carry information about the true jet momentum, the calorimeter is much better at measuring the total energy of the jet. This is because the Inner Detector does not record neutral particles and its p_{T} resolution deteriorates at high momentum. Consequently we combine information from both tracks and calorimeter cells to estimate the true jet momentum. The negative impact of calorimeter failures on the quality of momentum reconstruction is characterized.

We use Monte Carlo events to study two separate damage scenarios:

1. A high-voltage power supply of LAr fails, creating a "blind spot" in LAr that spans $0 < \eta < 1.4$ and $\frac{\pi}{4} - \frac{\pi}{16} < \phi < \frac{\pi}{4} + \frac{\pi}{16}$ (i.e. $\Delta\phi = 22.5°$).
2. The super-drawer reading out TileCal module LBC13 fails, causing a "blind spot" that spans $-1 < \eta < 0$ and $\frac{12\pi}{32} < \phi < \frac{13\pi}{32}$ (i.e. $\Delta\phi = 5.6°$).

In Section 2 we describe the Monte Carlo datasets and the software used to simulate the effect of the defective calorimeter regions. The algorithms used to reconstruct truth jets, calorimeter jets, and track jets are discussed in Section 3; the resulting efficiency and purity are shown in Section 4. Section 5 describes a way to estimate the true jet momentum based on track jets and surviving information from the damaged calorimeter. The performance of track jets and calorimeter jets are compared in each of the aforementioned damage scenarios.

2 Datasets and Software

For this study we used approximately 400K events from each of the dijet ESD datasets listed in Table 1. These were generated using Pythia 6.415.2 in Athena release 14.2.0.1 as part of the `mc08` production at $\sqrt{s} = 14$ TeV. They were simulated, digitized, and reconstructed in release 14.1.0.3 with detector geometry `ATLAS-CSC-05-01-00`.

Dataset	p_{T} bin	Events used
`mc08.105009.J0_pythia_jetjet.recon.ESD.e344_s456_r456`	8-17 GeV	395K
`mc08.105010.J1_pythia_jetjet.recon.ESD.e344_s456_r456`	17-35 GeV	391K
`mc08.105011.J2_pythia_jetjet.recon.ESD.e344_s456_r456`	35-70 GeV	389K
`mc08.105012.J3_pythia_jetjet.recon.ESD.e344_s456_r456`	70-140 GeV	383K
`mc08.105013.J4_pythia_jetjet.recon.ESD.e344_s456_r456`	140-280 GeV	379K
`mc08.105014.J5_pythia_jetjet.recon.ESD.e344_s456_r456`	280-560 GeV	379K
`mc08.105015.J6_pythia_jetjet.recon.ESD.e344_s456_r456`	560-1120 GeV	380K
`mc08.105016.J7_pythia_jetjet.recon.ESD.e344_s456_r456`	1120-2240 GeV	301K

Table 1: Dijet ESD datasets listed along with p_{T} cut on leading two partons.

Re-reconstruction from ESD was performed using `RecExCommon-00-09-57` (`Reconstruction/RecExample/RecExCommon`) in the AtlasProduction-14.2.20.3 cache of Athena. In addition, it was patched with updated versions `CaloRec-02-08-37` (`Calorimeter/CaloRec`) and `MissingET-03-01-19-01` (`Reconstruction/MissingET`) that contain needed fixes for cluster, jet, and $E_{\mathrm{T}}^{\mathrm{miss}}$ rebuilding. The ESD re-reconstruction was run via distributed analysis jobs on PanDA [4].

Calorimeter cells (`CaloCells`) in the defective LAr or TileCal region were assigned zero energy. Then 4-2-0 `CaloTopoClusters` were rebuilt on-the-fly from the modified `CaloCells` and calibrated using the H1 calibration scheme. Calorimeter (`Cone4H1TopoJets`) jets were rebuilt from the new topoclusters using the "standard" ATLAS fixed cone jet finder with a radius of 0.4. Lastly the $E_{\mathrm{T}}^{\mathrm{miss}}$ (`MET_RefFinal`) was rebuilt using the new clusters and jets, although it was not studied in this note.

As a consistency check of the re-reconstruction, negligibly small differences were observed between the pre-existing topoclusters stored in the ESD and those rebuilt from unmodified ESD `CaloCells`. These minute differences were traced to the fact that the pre-existing topoclusters were built during reconstruction from the original `CaloCells` in the RDO, whereas the cluster rebuilding was performed with `CaloCells` in the ESD that have been compressed with a lossy algorithm that only stores cells above a given threshold. [5]

3 Jet Finding

3.1 Truth Jets

The truth jets considered in this study are taken from the `Cone4TruthJets` container. These were built from `TruthParticles` in the `INav4MomTruthEvent` container using the "standard" ATLAS fixed cone jet finder [6], an iterative seeded cone algorithm with seed $p_{\mathrm{T}} > 1$ GeV. A radius $\Delta R = \sqrt{\Delta\eta^2 + \Delta\phi^2} = 0.4$ was used along with a split-merge fraction of 0.5.

3.2 Calorimeter Jets

The calorimeter jets are taken from the `Cone4H1TopoJets` container. These jets were reconstructed using the same ATLAS cone jet finder with radius $\Delta R = 0.4$ that was used to create the truth jets above. However, these calorimeter jets were built from uncalibrated 4-2-0 `CaloTopoClusters`, whose energies were subsequently corrected according to cell energy density using the H1 global calibration [7]. Each uncalibrated 4-2-0 topocluster is seeded by a cell whose energy exceeds 4 times the cell-level noise (signal significance greater than 4); all of the seed's nearest neighbors are added; next-to-nearest neighbors with a signal significance greater than 2 are added; and finally a ring of guard cells is added as well. [8]

3.3 Track Jets

In this study we built track jets by clustering tracks using an iterative seeded cone algorithm of radius $\Delta R = 0.4$, similar to that used for truth jets and calorimeter jets. However, no split-merge was performed.

A simple preselection was imposed on tracks from the `TrackParticleCandidate` container before clustering them together. Tracks constructed exclusively from Transition Radiation Tracker (TRT) hits are assigned disingenuous pseudorapidity (η), since drift tubes in the TRT barrel are aligned longitudinally along the z axis.[1] Consequently we removed such tracks by requiring at least 4 silicon hits, which may come from either the Pixel Detector or the Silicon Central Tracker (SCT). No cuts on d_0 nor on $z_0 \sin\theta$ were imposed to remove secondaries and conversions.

[1] In the TRT Barrel, the assigned η is determined by the geometric center of the middle straw with respect to the reconstructed vertex. In the endcaps, the first or last straw can be used.

The clustering of preselected tracks into track jets proceeds according to the following algorithm. First, all tracks are sorted descending by p_{T}. Tracks with $p_{\mathrm{T}} > 1$ GeV may be used as seeds. The algorithm starts from the highest-p_{T} seed available, and goes through the p_{T}-ordered list of tracks that have not yet been clustered. A track is clustered with the seed at hand if it lies within $\Delta R < 0.4$ from it and its associated reconstructed vertex is within $\Delta z < 1$ mm from the vertex of the seed. The momentum of the cluster is recalculated each time a new track is added to it, and the next track to be added must lie within $\Delta R < 0.4$ of the direction of the updated cluster momentum. Once the list of tracks is exhausted, the cluster is complete and is defined as a reconstructed track jet. The algorithm then repeats the process with the next highest p_{T} seed available, iterating until there are no seeds left. Track jets with fewer than 3 tracks or that have $\sum p_{\mathrm{T}} < 5$ GeV are discarded.

4 Efficiency and Purity

To assess how well track jets and calorimeter jets perform with respect to truth-level jets, we use the standard definitions of purity and efficiency:

$$\text{purity} \equiv \frac{\text{Reconstructed jets that match a truth jet}}{\text{Reconstructed jets}}, \tag{1}$$

$$\text{efficiency} \equiv \frac{\text{Truth jets matched by a reconstructed jet}}{\text{Truth jets}}, \tag{2}$$

where a reconstructed jet and a truth jet "match" if their momenta point within $\Delta R < 0.2$ of each other. Track jets are compared to calorimeter jets within the Inner Detector acceptance of $|\eta| < 2.5$.

Fig. 1 shows the purity and efficiency of track and calorimeter jets as a function of momentum p and detector η and ϕ in the case of a fully functional calorimeter. Track jets perform as well as calorimeter jets in terms of purity, while they become less efficient at $|\eta| > 1.5$.

A calorimeter failure does not affect the track jet efficiency and purity because they do not rely on the calorimeter. However calorimeter jet performance will be degraded. In the rest of this section we compare calorimeter jet efficiency and purity to those of track jets in the damage scenarios described in Section 1.

Fig. 2 shows the first scenario described in Section 1, in which a LAr high-voltage power supply (HVPS) fails. In the defective region, calorimeter jets are less efficient but more pure than with the healthy detector. This is because the damage greatly lowers their reconstruction efficiency, but also somewhat reduces the likelihood of reconstructing a spurious jet. Fig. 3 shows the same scenario of a dead LAr HVPS, but where purity and efficiency are now calculated using only jets in the damaged LAr region. Isolating the problematic region better illustrates the effect of the damage. Note that the calorimeter jet efficiency rises with increasing true jet momentum due to the larger fraction of energy deposited in TileCal behind the defective LAr region.

Fig. 4 shows the second scenario described in Section 1, in which a TileCal barrel module fails. This is a less serious case because the $\eta - \phi$ area of this Tile defect is approximately $\frac{1}{6}$ the size of the LAr damage in the previous scenario. Furthermore, TileCal records the tail-end of showers, thus providing less critical information than LAr. For these reasons the efficiency and purity of calorimeter jets in the harmed region are not affected much.

5 Jet Momentum Estimation

We would like to calibrate the momentum of the track jets that we have reconstructed in Section 3.3 to use as an estimator for the true jet momentum. An elaborate scheme analogous to H1 global calibration could

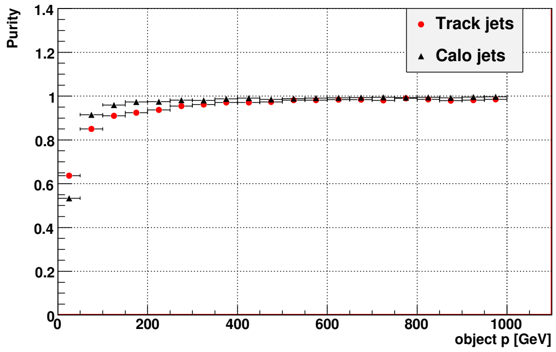

(a)

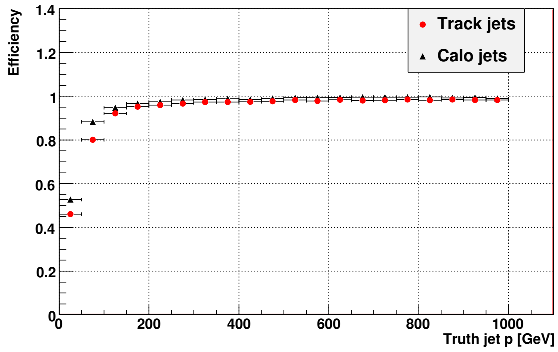

(b)

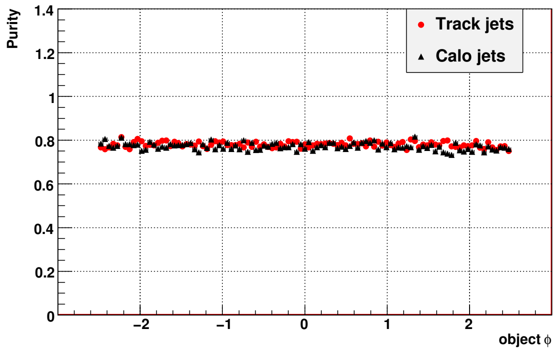

(c)

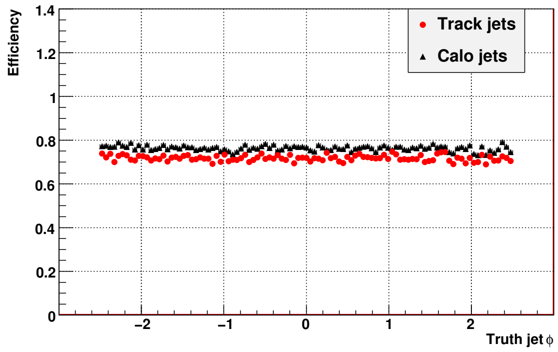

(d)

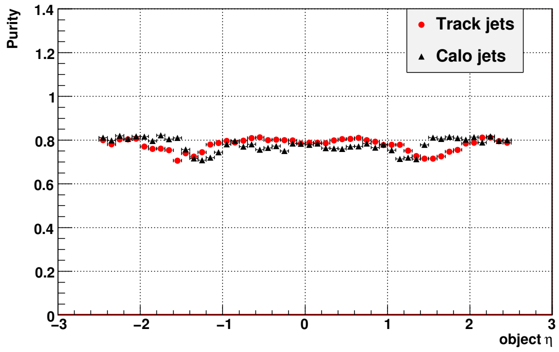

(e)

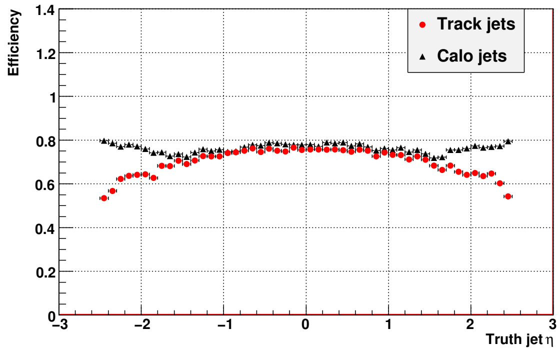

(f)

Figure 1: Purity and efficiency of track and calorimeter jets in the absence of calorimeter damage as a function of momentum p (1(a) and 1(b)), of ϕ (1(c) and 1(d)), and of detector η (1(e) and 1(f)). In Fig. 1(a), "object p" corresponds to H1 corrected momentum for calorimeter jets, while for track jets it is simply the total track momentum. Hence the two plots in 1(a) are not directly comparable, but are plotted together with this caveat explicit.

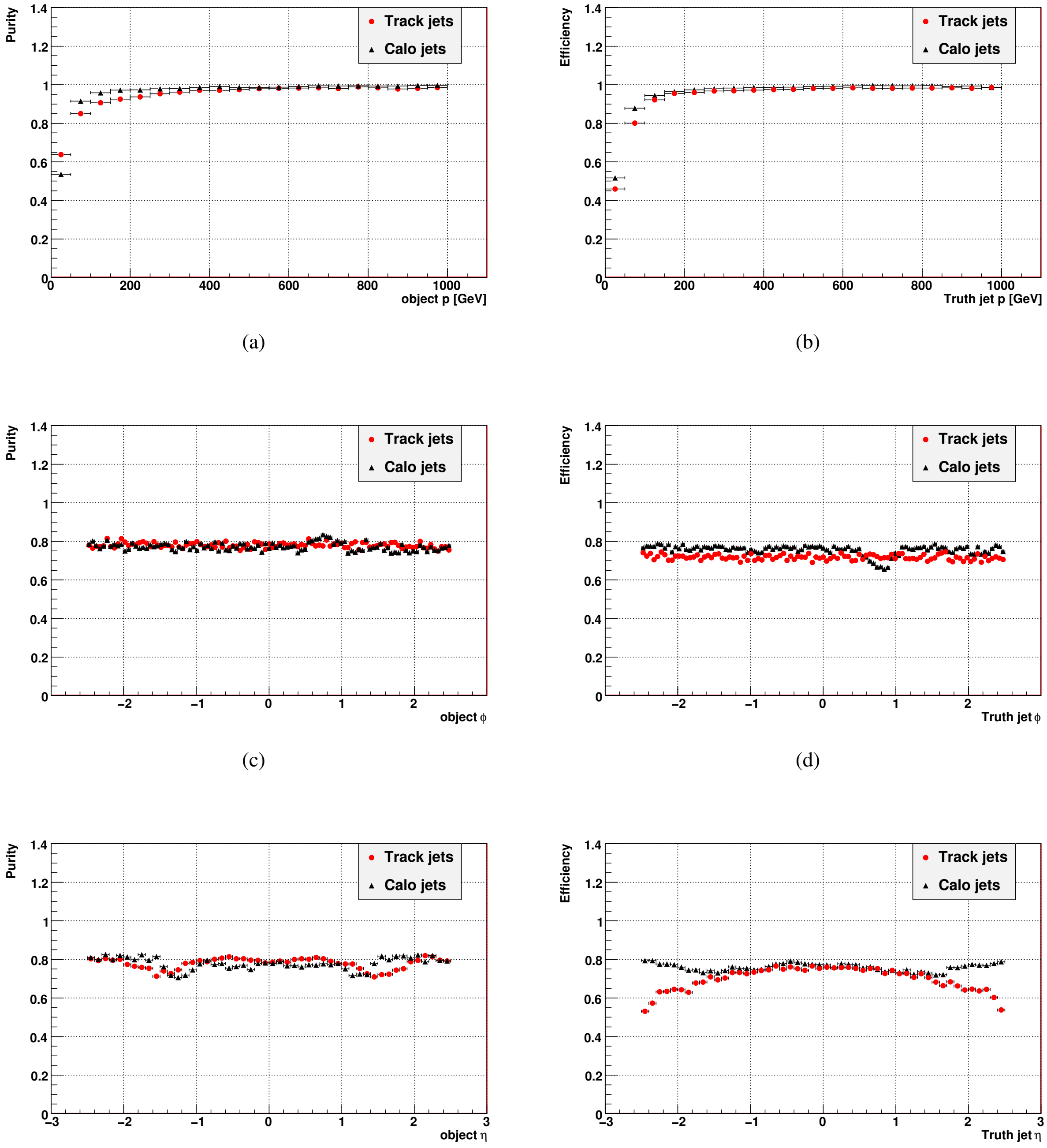

(a) (b) (c) (d) (e) (f)

Figure 2: Same as Fig. 1, but with the LAr HVPS failure described in Section 1. All true and reconstructed jets within $\eta < 2.5$ and at any ϕ are included, not just those in the damaged region.

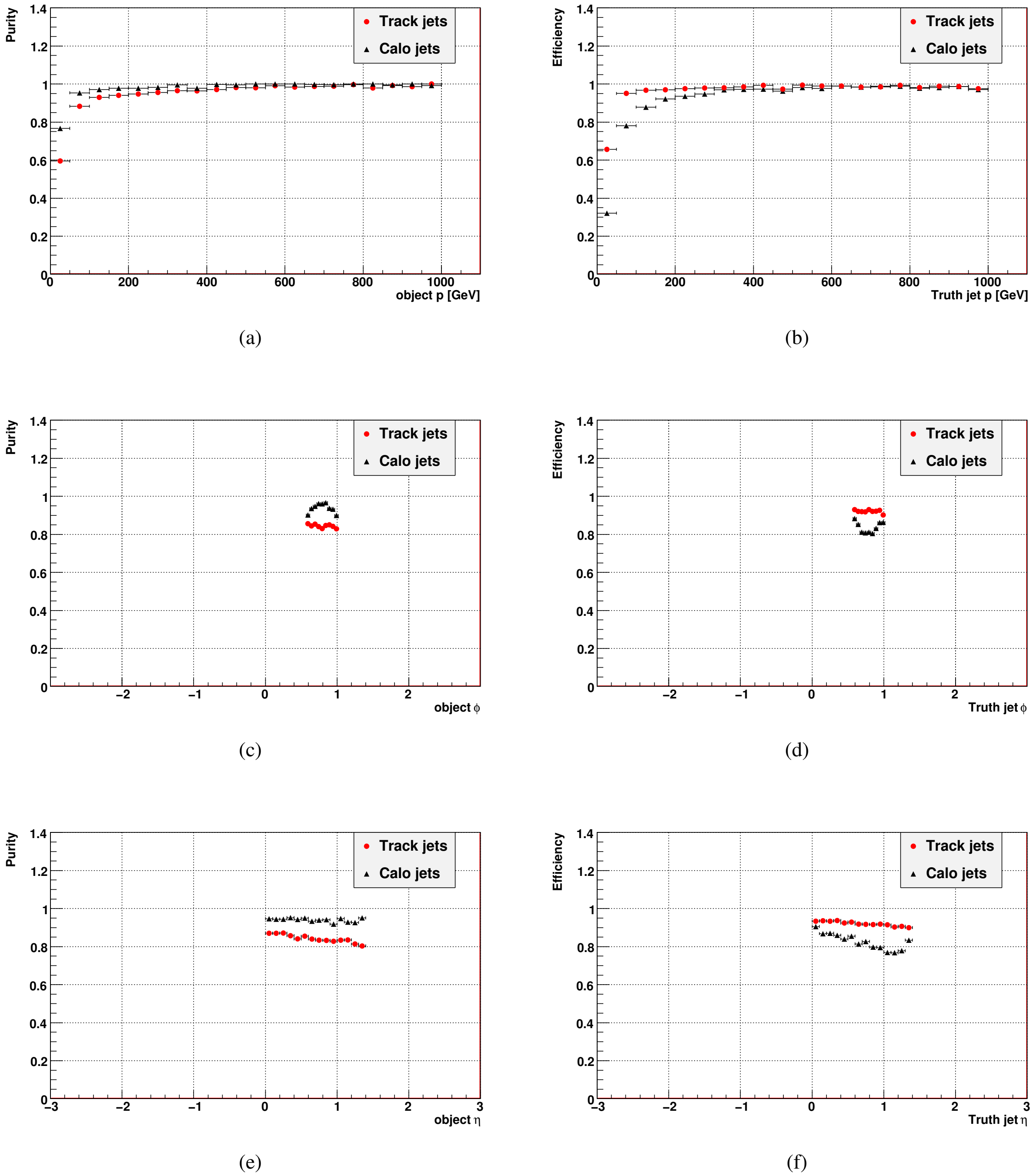

Figure 3: Same as Fig. 1, but with the LAr HVPS failure described in Section 1. Only true and reconstructed jets from the damaged region are considered, which is why the effect of the damage appears more clearly than in Fig. 2.

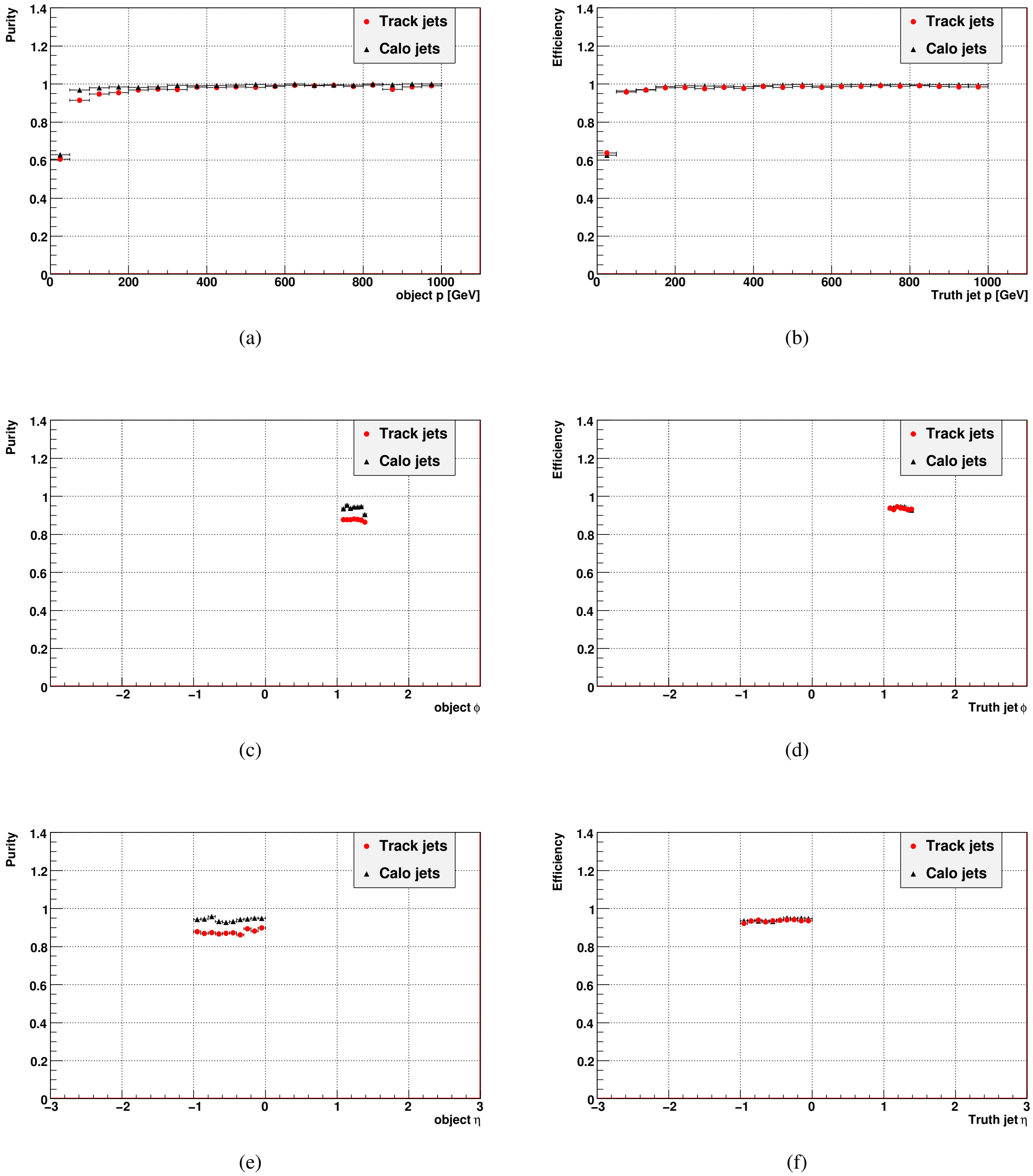

Figure 4: Same as Fig. 1, but with the Tile barrel module failure described in Section 1. Only true and reconstructed jets from the damaged region are considered. The damage is not serious enough to significantly reduce the efficiency of calorimeter jets.

be invented and tuned specifically for problematic detector regions, but this would likely be overkill in the case of a damaged calorimeter. Instead we have developed a simple calibration scheme that is tuned for local use in the damaged region. It exploits a couple observables of the track jet without scrutinous cell-level optimization.

The calibration first selects track jets centered in the problematic region that match a truth jet. We correlate the momentum of the truth jet to the following observables of the corresponding track jet:

1. The EM-scale calorimeter energy within a cone of $\Delta R < 0.4$ around the track jet's momentum.

2. The magnitude of the track jet momentum, namely $|\sum \vec{p}|$ where the summation is taken over the constituent tracks belonging to the track jet.

This list of observables is not exhaustive. For example, we also considered as a third observable the angular separation between the two highest p_T tracks in the track jet (ΔR_{12}). However, we found that ΔR_{12} had a negligible effect on the performance of the estimator we were trying to construct. One could also consider counting the hits in the muon chambers aligned with the track jet, although we did not involve the Muon Spectrometer [9] in this study.

From the calorimeter energy within a track jet, we obtain from Monte Carlo a prediction of the true jet momentum along with its uncertainty. The $|\sum \vec{p}|$ of the track jet provides a separate prediction of the true momentum. To obtain a final estimator of the truth-level momentum, we average the above two predictions, weighting them inversely to their respective variances under the assumption that they are uncorrelated.[2]

Fig. 5 shows the dependence of true momentum on the two observables used. Comparing for example Fig. 5(a) to 5(b) for a healthy detector, we see that the prediction from the calorimeter energy has a smaller uncertainty than that from the track jet momentum.[3] Since we use the weighted average of the two predictions as our final estimate, the prediction from the calorimeter energy dominates. This changes when the calorimeter is sufficiently damaged that it contributes about as much precision as the Inner Detector. Such an example is the scenario in which a dead LAr high-voltage power supply dies, which is shown in Fig. 5(c) and 5(d). An intermediate case is the scenario when a Tile barrel module fails.

The bias and resolution of the track jet estimator with respect to truth jets is shown in Fig. 6 for the different scenarios of calorimeter damage. They are compared to calorimeter jets under the same conditions. Fig. 6 is constructed using the mean and standard deviation found from Gaussian fits such as those shown in Fig. 7 (healthy detector), 8 (dead LAr HVPS), and 9 (dead Tile module).

Fig. 6(b), which corresponds to a healthy detector, shows that the momentum predicted by track jets is slightly less precise than that of the H1 calibrated topocluster jets. This is not surprising since the H1 calibration scheme exploits cell-level information via dedicated corrections for each cell, whereas the estimator introduced here uses only two observables (calorimeter energy and track momentum within the track jet) that are averaged over the whole $\eta - \phi$ region to translate them to true jet momentum.

Fig. 6(c) and 6(d) show that, in the region of a LAr HVPS failure, the momentum estimated from track jets is less biased and has better resolution at high true jet momentum. Also recall that, as shown in Fig. 3, track jets are more efficient at identifying jets in that kinematic region in the presence of LAr damage.

[2]This non-trivial point was given the necessary attention. For instance, before deciding to use the calorimeter energy within the track jet as an observable, we experimented with using the separate LAr and TileCal energies within the track jet. However, as expected those two observables were found to be strongly anti-correlated for a given true jet momentum. Due to this anti-correlation, the calorimeter energy provides a truth-level momentum estimator of much smaller variance than either LAr or TileCal alone. Unlike the case of separate LAr and TileCal predictions, the correlation factor between the calorimeter energy and the track jet momentum $|\sum \vec{p}|$ was found to be less than 2% on average, so we ignore it.

[3]This is expected, otherwise one wouldn't need a calorimeter to measure jet energy.

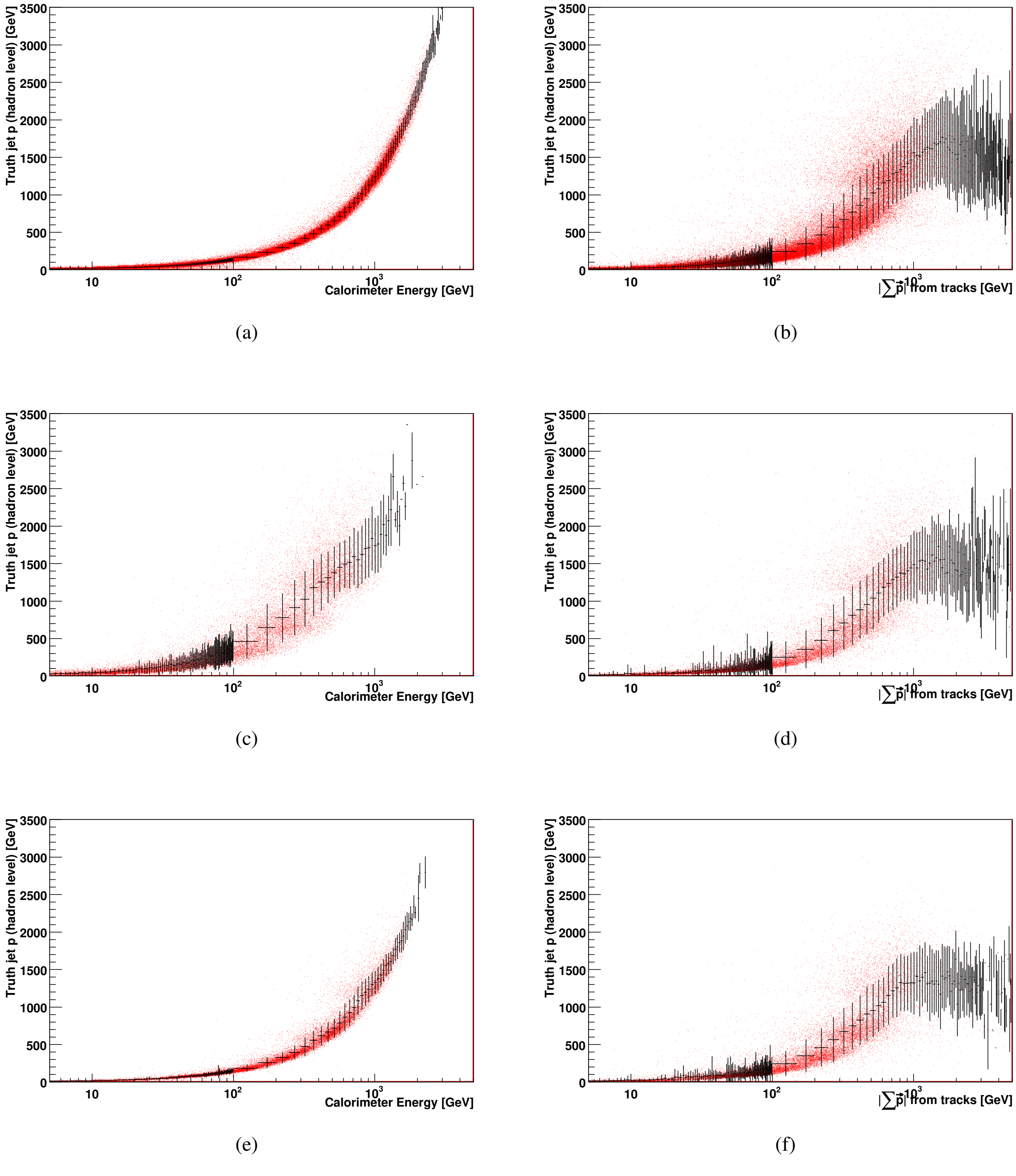

Figure 5: The momentum of the matching truth jet is shown as a function of the calorimeter energy within $\Delta R < 0.4$ from the reconstructed track jet axis (left) and as a function of $|\sum \vec{p}|$ of tracks in the track jet (right). In 5(a) and 5(b) the calorimeter is fully functional and the whole $|\eta| < 2.5$ region is included. In 5(c) and 5(d) a LAr HVPS is dead and only jets from the damaged region are used. In 5(e) and 5(f) a Tile barrel module is dead and only jets from the damaged region are used. The red points illustrate the 2D scatter plot; the black points and error bars indicate the mean and RMS, respectively, of the associated profile obtained by averaging over the y-axis bins for each x-axis bin.

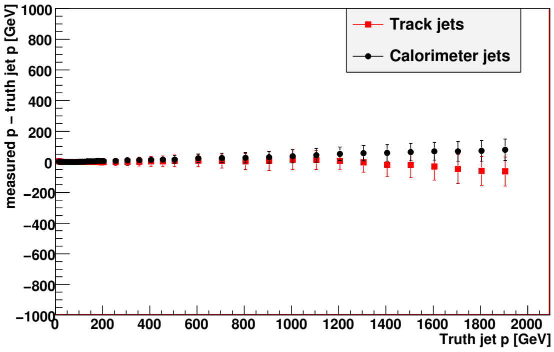

(a)

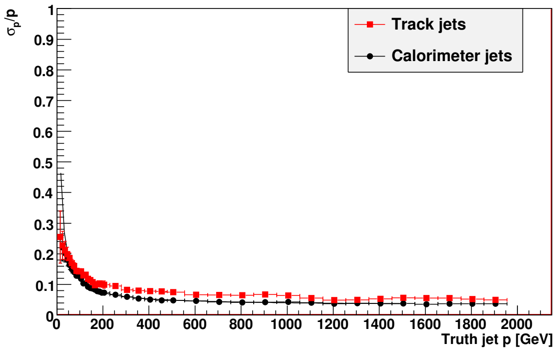

(b)

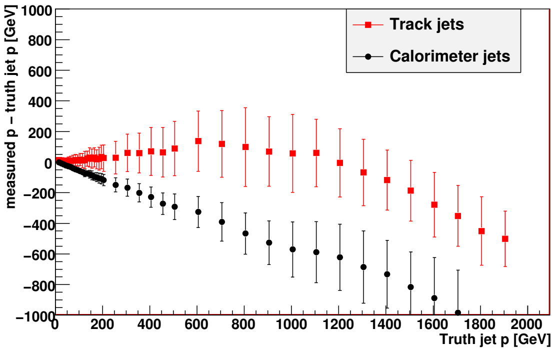

(c)

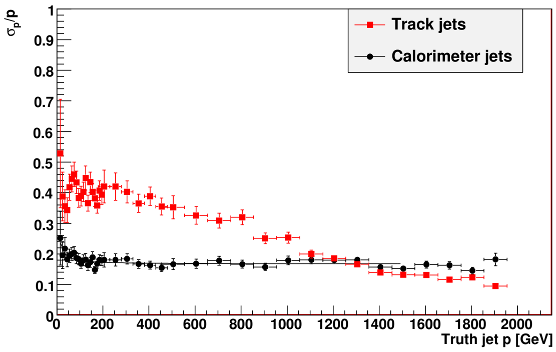

(d)

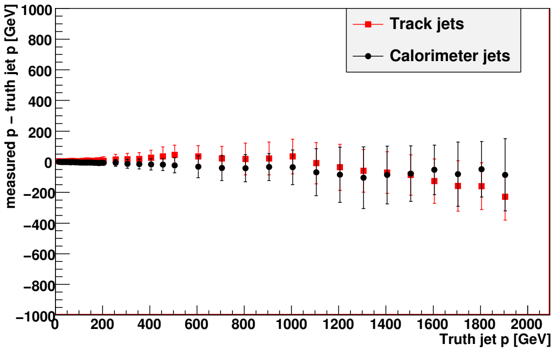

(e)

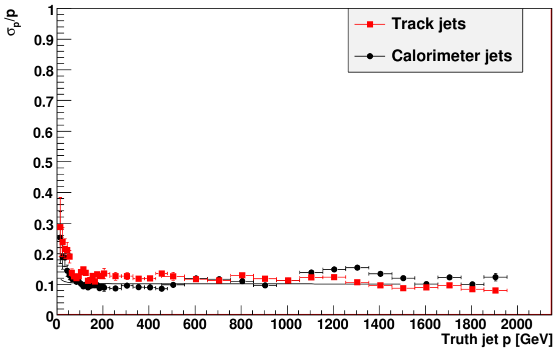

(f)

Figure 6: Difference between predicted and true momentum (left) and relative uncertainty of prediction, i.e. resolution (right). The prediction described in the text (red) is compared to that of calorimeter jets derived with the H1 calibration. 6(a) and 6(b) correspond to no damage, and include reconstructed jets from the whole $|\eta| < 2.5$ region that match a truth jet. 6(c) and 6(d) correspond to the case of a dead LAr HVPS, and include reconstructed jets centered in the damaged region that match a truth jet. The same applies to 6(e) and 6(f), only they correspond to the case of a dead Tile module.

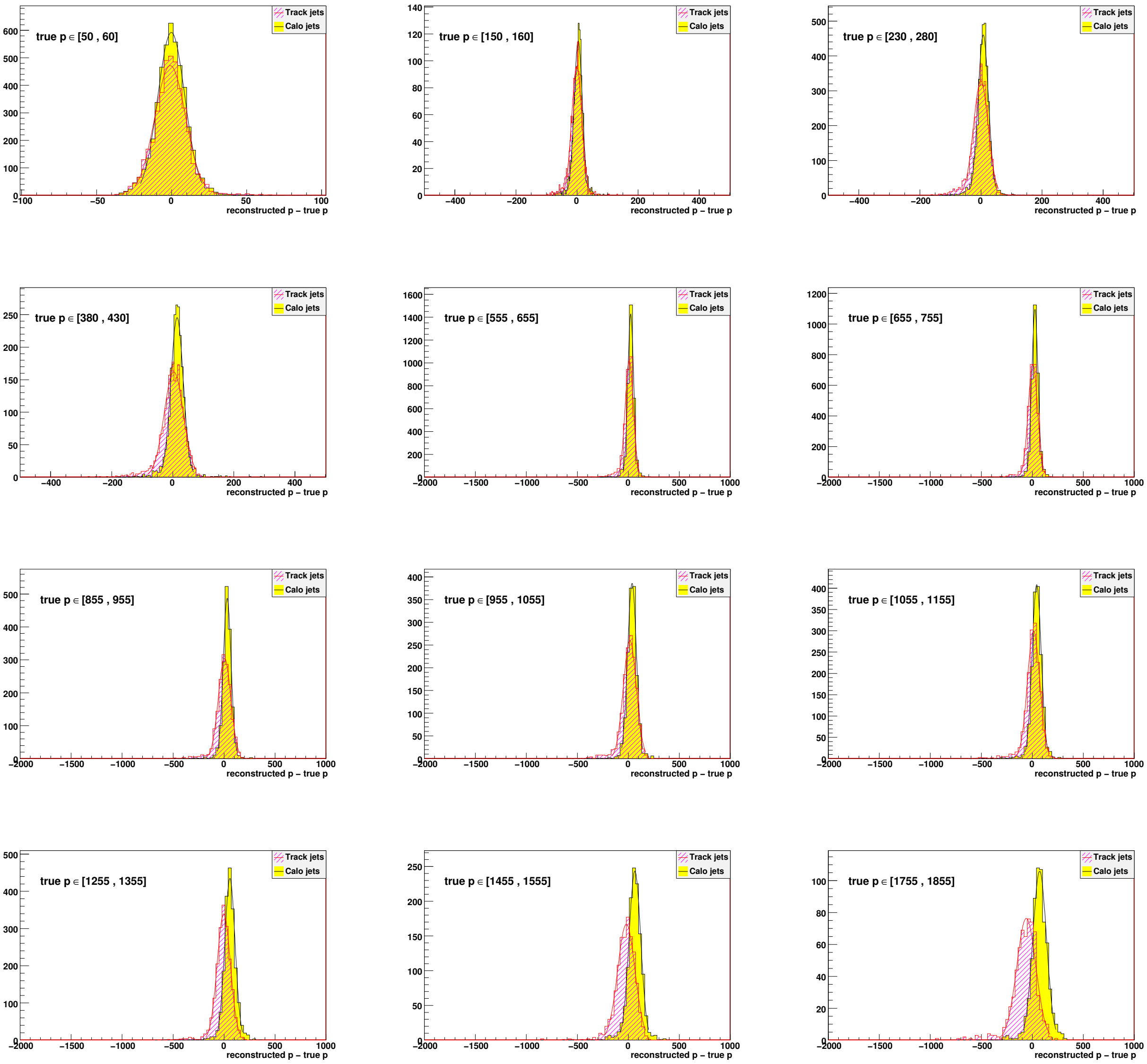

Figure 7: Difference between predicted and true momentum for reconstructed jets (track and topocluster jets) matching a truth jet, shown in various bins of true momentum. The distributions correspond to a healthy detector with jets from the whole $|\eta| < 2.5$ region.

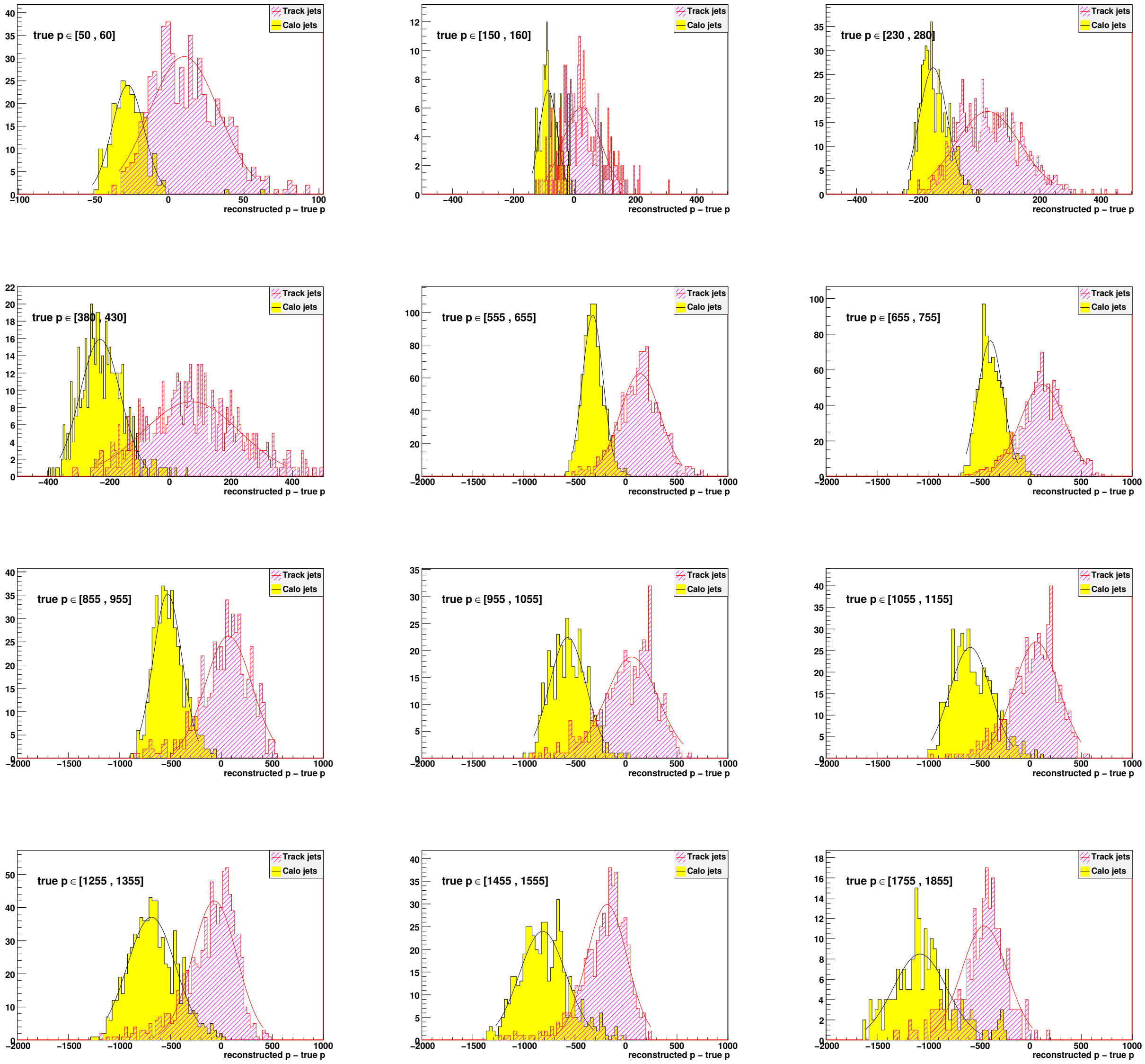

Figure 8: Same as Fig. 7. The distributions correspond to a dead LAr HVPS and consider only jets from the damaged region.

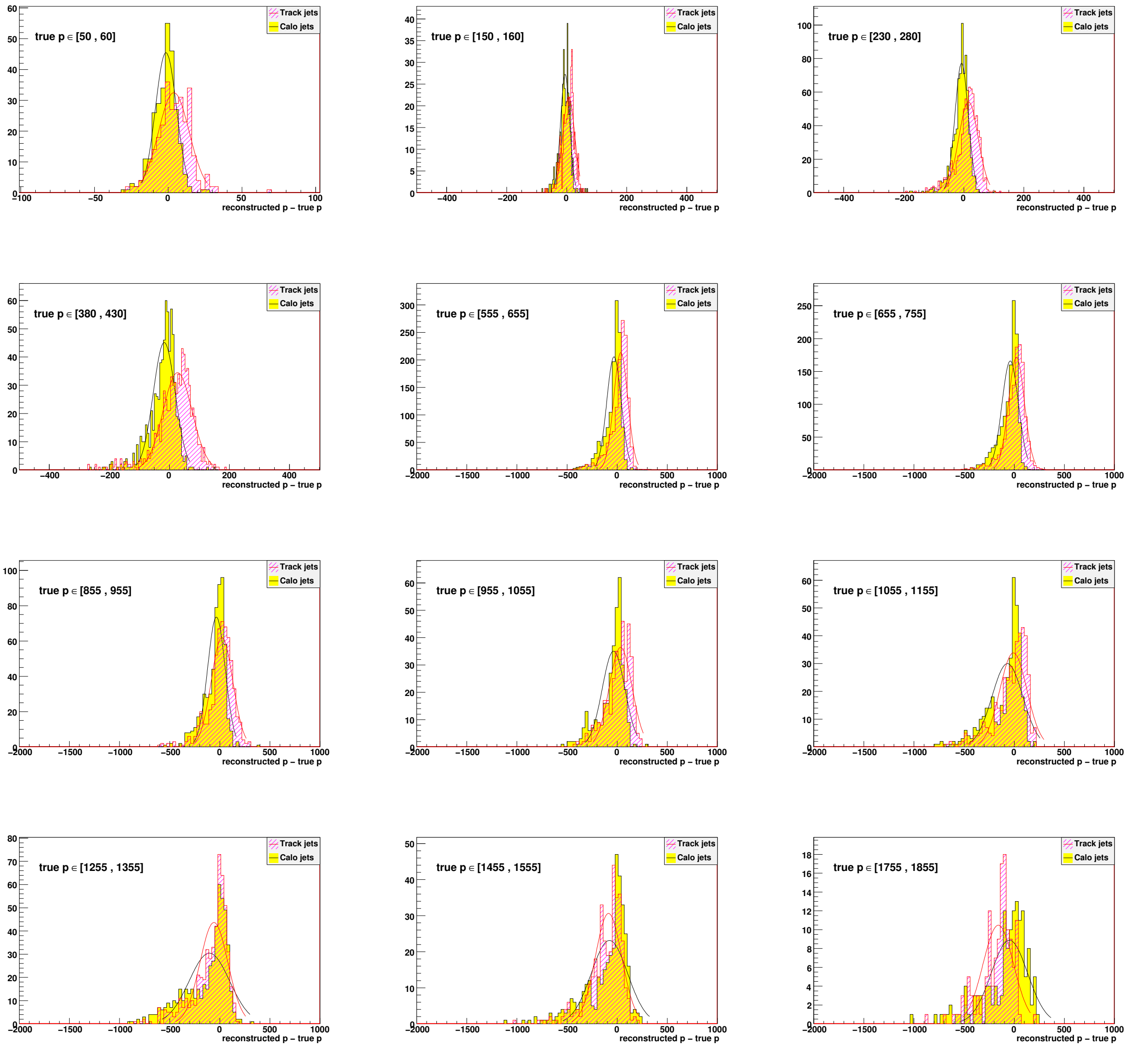

Figure 9: Same as Fig. 7. The distributions correspond to a dead Tile module and consider only jets from the damaged region.

Fig. 6(f) indicates that if a TileCal barrel module fails, the momentum resolution using track jets is comparable to that of calorimeter jets, providing a slight improvement above ~ 1 TeV. Because the damage is not severe enough to degrade the calorimeter jet reconstruction efficiency lower than that of track jets (see Fig. 4), in this scenario there is less benefit to using track jets.

6 Conclusion

We have investigated the option of reconstructing jets using tracks to address local calorimeter damage. It was found that in the case of significant LAr damage, such as the failure of a high-voltage power supply, the reduced efficiency of topocluster jets in the damaged region could be improved by track jets. By contrast, the loss of a superdrawer in TileCal would not be serious enough to render topocluster jets less efficient than track jets.

A simple, Monte Carlo based calibration scheme was developed, which was tuned and applied locally in the damaged region to estimate truth-level jet momentum from two observables: the calorimeter energy within a cone around the track jet, and the total momentum of the tracks constituting the track jet. In the case of LAr damage studied, the momentum linearity is improved by the use of track jets calibrated with this scheme. In either scenario of LAr or Tile damage, momentum resolution of jets above approximately 1 TeV is improved.

7 Future Steps

This study could be expanded in a variety of ways. Here is a non-exhaustive list of ideas:

- Examine more failure scenarios, for example local tracker failures, or LAr and TileCal failing at the same $\eta - \phi$ position.
- Study track jets in the presense of pile-up.
- Assess the impact of calorimeter damage on $E_{\mathrm{T}}^{\mathrm{miss}}$ and use track jets to improve $E_{\mathrm{T}}^{\mathrm{miss}}$ measurement.
- Account for the effect of calorimeter damage on the trigger. [10]

8 Acknowledgments

We wish to thank Jim Pilcher, David W. Miller, Ariel Schwartzman, Peter Onyisi, Martina Hurwitz, Frank Paige, Ambreesh Gupta, Frank Merritt, and Mark Oreglia for their constructive feedback. This work was funded by the National Science Foundation. GC thanks the Grainger Fellowship for support; EJF thanks the McCormick Fellowship and GAANN Fellowship for support.

References

[1] *ATLAS Tile Calorimeter: Technical Design Report*. Technical Design Report ATLAS. CERN, Geneva, 1996.

[2] *ATLAS Liquid-Argon calorimeter: Technical Design Report*. Technical Design Report ATLAS. CERN, Geneva, 1996.

[3] A. Andreazza, et al., *The Expected Performance of the ATLAS Inner Detector*, Tech. Rep. ATL-COM-PHYS-2008-105, CERN, Geneva, Aug, 2008.

[4] International Conference on Computing in High Energy and Nuclear Physics (CHEP'07), *PanDA: Distributed Production and Distributed Analysis System for ATLAS*, vol. 119. 2008.

[5] S. Menke and G. L. Usai, *Proposal for Compactification of CaloCell Objects*, Tech. Rep. ATL-SOFT-2004-005. ATL-COM-SOFT-2004-007. CERN-ATL-COM-SOFT-2004-007, CERN, Geneva, 2004.

[6] ATLAS Collaboration, Proudfoot, J (Editor), and Mader, W F (Editor), *Jet, Missing Et and Tau Combined Performance*, Tech. Rep. ATL-COM-PHYS-2008-074, CERN, Geneva, May, 2008. p. 7.

[7] ATLAS Collaboration, *Expected Performance of the ATLAS Experiment, Detector, Trigger and Physics*, Tech. Rep. ATL-COM-PHYS-2008-243, CERN, Geneva, Dec, 2008. pp. 298-301.

[8] ATLAS Collaboration, Proudfoot, J (Editor), and Mader, W F (Editor), *Jet, Missing Et and Tau Combined Performance*, Tech. Rep. ATL-COM-PHYS-2008-074, CERN, Geneva, May, 2008. pp. 9-10.

[9] *ATLAS Muon Spectrometer: Technical Design Report*. Technical Design Report ATLAS. CERN, Geneva, 1997.

[10] D. Casadei, *HLT MET Trigger Slice: Study of Problems Due to Lost Power Supply*, ATLAS JetEtMiss Performance Meeting. August 20, 2008.